Effect of chemical defects on electrostriction-enhanced piezoelectric property of poly(vinylidene fluoride) via high-power ultrasonication

Guanchun Rui ¹, Elshad Allahyarov ^{2,3,4}, Honghu Zhang ⁵, Ruipeng Li ⁵, Shihai Zhang ⁶, Philip L. Taylor ^{2,*}, Lei Zhu ^{1,*}

¹ Department of Macromolecular Science and Engineering, Case Western Reserve University,

Cleveland, Ohio 44106-7202, United States

- ³ Institut für Theoretische Physik II: Weiche Materie, Heinrich-Heine Universität Düsseldorf,
 Universitätstrasse 1, 40225 Düsseldorf, Germany
- ⁴ Theoretical Department, Joint Institute for High Temperatures, Russian Academy of Sciences, 13/19

 Izhorskaya street, Moscow 125412, Russia
 - ⁵ National Synchrotron Light Source II, Brookhaven National Laboratory, Upton, New York 11973, United States

⁶ PolyK Technologies, LLC, State College, PA 16803, United States

² Department of Physics, Case Western Reserve University, Cleveland, Ohio 44106, United States

^{*} Corresponding authors. Emails: lxz121@case.edu (L. Zhu) and plt@case.edu (P.L. Taylor)

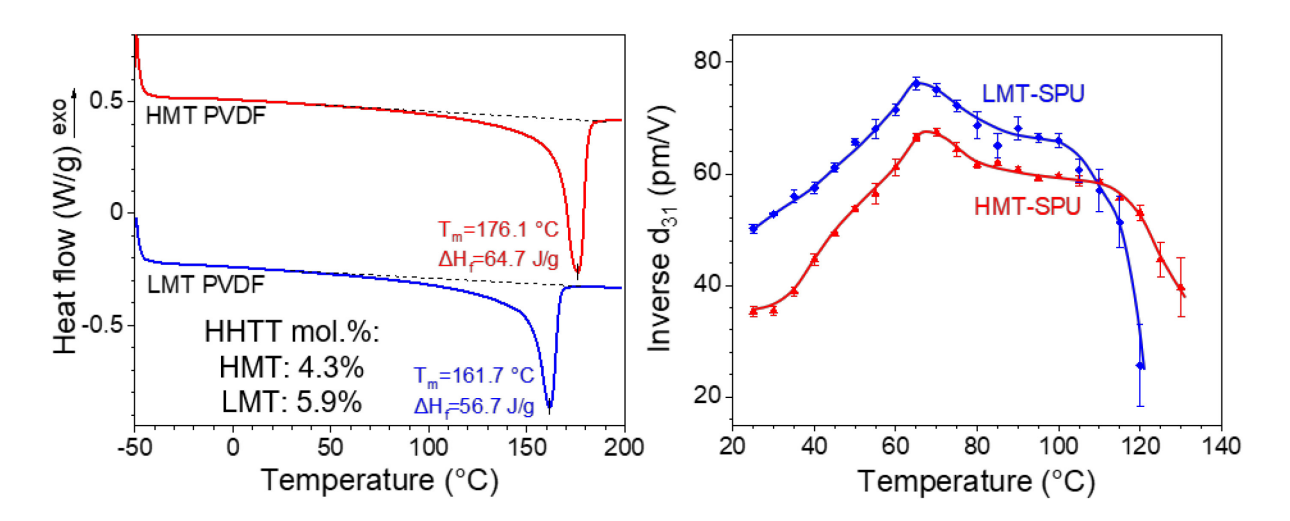
Abstract

Among all ferroelectric polymers, poly(vinylidene fluoride) (PVDF)-based polymers exhibit the best piezoelectric properties and thus are promising for sensors, actuators, and energy harvesters in flexible/wearable electronics and soft robotics. Despite decades of research effort, the structure-property relationship is still unclear for ferroelectric polymers, and their piezoelectric performance is often limited to ~30 pC/N. In this study, we report the effects of chemical defects [i.e., the head-to-head and tail-to-tail (HHTT) sequence] and high-power ultrasonication on the piezoelectric performance of PVDF. Two PVDF homopolymers with different HHTT contents were studied. The PVDF with a lower HHTT content (4.3%) exhibited a higher melting temperature (T_m, denoted as HMT), whereas that with a higher HHTT content (5.9%) exhibited a lower T_m (denoted as LMT). In addition to the primary crystals (PCs) and the isotropic amorphous fraction, wide-angle X-ray diffraction also suggested the presence of the oriented amorphous fraction (OAF) and secondary crystals (SCs), which are important in enhancing the piezoelectricity for PVDF. Intriguingly, the LMT PVDF exhibited higher piezoelectric performance than the HMT PVDF, because it had a higher OAF/SC content. In addition, high-power ultrasonication was shown to effectively break relaxor-like SCs off from the PCs, further enhancing the piezoelectric performance. That is, the inverse piezoelectric coefficient d₃₁ reached as high as 76.2 pm/V at 65 °C for the ultrasonicated LMT PVDF. The insight from this study will enable us to design better piezoelectric PVDF polymers for practical electromechanical applications.

Keywords

Electrostriction; Piezoelectricity; Poly(vinylidene fluoride); Chemical defects; High-power ultrasonication

TOC Graphic



1. Introduction

Among all ferroelectric polymers, poly(vinylidene fluoride) (PVDF) and its random copolymers, such as P(VDF-co-trifluoroethylene) [P(VDF-TrFE)], exhibit the best piezoelectric performance.[1, 2] Much fundamental and applied research effort has been dedicated to this field since piezoelectricity in PVDF was discovered by Kawai in 1969.[3] However, typical piezoelectric coefficients (d_{3j} , j = 1, 2, 3 for the stretching, transverse, and thickness directions) of PVDF-based ferroelectric polymers remain in the range of 10-30 pC/N, despite of numerous attempts at improvement over the past five decades.[4-8] Moreover, even the origin of piezoelectricity in ferroelectric polymers is still at a point of discussion.

According to Broadhurst,[9] the direct piezoelectric charge constants d_{3j} can be rewritten as:

$$d_{3j} = P_{r0} \left(\frac{\partial ln M_3}{\partial T_j} - \frac{\partial S_3}{\partial S_j} J_j \right) \tag{1}$$

where P_{r0} is the permanent remanent polarization in the thickness direction, M_3 is the macroscopic dipole moment in the poled sample, T_j is the applied stress, S_j is the electromechanical strain, and J_j is the compliance. Based on this equation, the piezoelectricity comes from three variables in the equation. First, P_{r0} is obtained from the macroscopically poled crystalline β phase in PVDF. In general, the higher P_{r0} the higher direct d_{3j} . Recently, a high P_{r0} of 120 mC/m² was reported for a biaxially oriented PVDF (BOPVDF) film, and a high direct d_{33} up to -62 pC/N was obtained.[10] Second, the compliance J_j plays an important role in soft polymers, as opposed to hard inorganic piezoelectrics. It is largely related to the dimensional effect, which describes the change of the dipole moment density upon the application of a stress.[9, 11-13] For example, a semicrystalline ferroelectric polymer can be considered as a model of hard crystals with rigid dipoles dispersed in a soft and compressible amorphous matrix. When an external stress is applied, the dipole moment

density changes due to the compressibility of the amorphous phase. Studies have shown that the dimensional effect can account for nearly 50% of the observed d₃₃, but not as much for the d₃₁.[14] Therefore, the dimensional model cannot fully explain the piezoelectricity of ferroelectric polymers.

Third, the $\partial(\ln M_3)/\partial T_j$ term describes the change of the macroscopic dipole moment when an external stress is applied. It is considered to relate principally to the electrostriction effect (refer to our recent publication for the explanation of electrostriction in dielectric polymers[15, 16]). As pointed out by Furukuwa, et al., electrostriction is the origin of piezoelectricity for ferroelectric materials.[17] In other words, piezoelectricity is simply electrostriction under a bias polarization, P_{r0} :[18, 19]

$$S_i = 2Q_{3i}P_{r0}P_3 \tag{2}$$

where Q_{3j} is the electrostriction coefficient and P_3 is the applied polarization in the thickness direction. Because $P_3 = \varepsilon_0(\varepsilon_{r-1})E_3$, where ε_0 and ε_r are vacuum and relative permittivity and E_3 is the applied electric field along the thickness direction, Eqn. (2) can be rewritten as:

$$S_j = 2\varepsilon_0(\varepsilon_r - 1)Q_{3j}P_{r0}E_3 \tag{3}$$

From the definition of inverse piezoelectricity, $S_i = d_{ij}E_3$, we can obtain the piezoelectric coefficient:

$$d_{ij} = 2\varepsilon_0(\varepsilon_r - 1)Q_{3j}P_{r0} \tag{4}$$

From this equation, we clearly see that piezoelectricity is the electrostriction under a bias remanent polarization P_{r0} . However, it is still unclear where the piezoelectricity comes from for semicrystalline ferroelectric polymers. Is it the amorphous phase, the crystal, or the crystalline-amorphous interface? Given the low T_g of -45 °C,[20] the isotropic amorphous phase of PVDF cannot keep its dipole orientation at room temperature. Therefore, piezoelectricity should not be expected to come from the isotropic amorphous phase in PVDF. Recently, Liu et al. discovered the

morphotropic phase boundary (MPB)-like behavior for P(VDF-TrFE) random copolymers with a composition near 50/50 mol.%.[21-24] It was considered that the conformation transformation of P(VDF-TrFE) chains in the primary crystals (PCs) from the 3₁ helical to the all-trans conformation accounted for the enhanced piezoelectricity (inverse $d_{33} = -62.5 \text{ pC/N}$). However, this mechanism cannot explain the piezoelectricity for PVDF homopolymers with a pure β phase. In 1980, Tashiro et al. proposed that the mechanical and electric heterogeneity between the amorphous and crystalline phases should be used to explain the high d₃₁ of uniaxially stretched PVDF.[14] Tasaka and Wada proposed that the high Poisson ratio and thus the orientation of the amorphous phase in stretched PVDF films were the origin of piezoelectricity.[25-27] However, they did not point out where the oriented amorphous phase is in semicrystalline PVDF. Later, the piezoelectricity of PVDF-based polymers was attributed to the coupling at the crystalline-amorphous interfaces. [28, 29] However, this coupling effect was not well-articulated. Recently, we pointed out that this coupling effect was realized through the oriented amorphous fraction (OAF), which linked between the PC lamella and the isotropic amorphous fraction (IAF).[10, 30-32] Namely, the electrostriction of the OAF induced the electro-actuation and thus piezoelectricity of PVDF.[31, 33] Note that the complex semicrystalline structure of PVDF cannot be explained by the simple two-phase model. If polarizable secondary crystals (SCs) could grow in the OAF layer of a P(VDF-TrFE) copolymer with composition around 50/50 mol.%, the piezoelectricity could be further enhanced.[31] Note that the extended-chain crystal (ECC) structure was important for the growth of the SCs in the OAF layer (i.e., SC_{OAF}), which could be achieved by annealing the P(VDF-TrFE) copolymers above their T_C.[34-36] However, P(VDF-TrFE) copolymers with a composition around 50/50 mol.% have a low Curie temperature (T_C) of ca. 65 °C,[37-39] above which the piezoelectricity will disappear when the P_{r0} decreases to zero for the paraelectric phase. In terms

of high temperature stability, PVDF homopolymers are more advantageous than P(VDF-TrFE) copolymers with a composition around 50/50 mol.%, because their T_C is above the melting temperature (T_m) at ambient pressure.[40]

In addition, the piezoelectric performance of P(VDF-TrFE) with a high VDF content is often poorer than that of PVDF.[31] More importantly, the current price of P(VDF-TrFE) copolymers is about 800 times higher than that of PVDF. Although P(VDF-TrFE) seems more advantageous than PVDF because it can directly crystallize into the ferroelectric phase without any post-treatments such as mechanical stretching or electric poling, PVDF is more practical for the ultimate commercialization. Ohigashi and coworkers reported high piezoelectric performance for high pressure-crystallized PVDF homopolymers with β-form ECCs.[41] We consider that the working mechanism should be attributed to the SCs in the OAF of the ECC PVDF. However, it is not practically possible to obtain uniaxially oriented PVDF films from high-pressure crystallization.

Other than neat ferroelectric polymers, polymer/piezoceramic composites have been considered to enhance the piezoelectric performance for polymers, because piezoceramics have much higher piezoelectric coefficients. However, the situation is not that simple for different types of composites. This is largely related to the electric poling process to achieve the macroscopic dipole moment for ferroelectric piezoelectrics. For composites without the parallel model structure, the electric field distribution is non-uniform.[42-44] For example, in a 0-3 composite, the high-permittivity (κ) fillers will have a low local field and the low-κ polymer matrix will have a high local electric field. When the permittivity contrast is large, the local field in the high-κ ceramic fillers is so low that ferroelectric switching is largely prohibited. Therefore, the polarizations in piezoceramic fillers remain random and they will not contribute much to the overall piezoelectric

performance.[45, 46] Only for composites with a parallel model structure, e.g., vertical 1-3 and 2-2, and 3-3 composites, where the electrode directly contacts the penetrating piezoceramic domains, the local electric field in the piezoceramics is high to induce the macroscopic dipole moment for piezoelectricity. Consequently, high piezoelectric performance is obtained.[45, 47-49] However, the piezoelectric coefficients are usually smaller than those of bulk piezoceramics. The advantage is that the 3-3 composites are not easy to break under large deformation with reasonably high piezoelectric performance.

In some studies, conductive fillers, such as carbon nanotubes and graphenes, are added into PVDF to enhance the piezoelectric performance.[50] However, like other power generators such as batteries and capacitors, internal conduction is detrimental to piezoelectricity because the generated charges can leak through the internal conductive pathways. This has been reported and discussed in the past.[4, 51, 52] Note, for direct piezoelectric measurements, triboelectricity during mechanical compression can also contribute to the generated charge and voltage, making the apparent piezoelectric coefficients appear to be high.[53] We consider that the enhanced piezoelectric performance for PVDF/carbon nanotube or graphene nanocomposites could be attributed to the triboelectric charge generation during direct d₃₃ measurements.

Another method to increase the piezoelectric coefficient is to utilize electrospun PVDF nanofibers.[54] As a result of high-voltage electrospinning, the deposited PVDF nanofiber mats exhibit self-polarization with a macroscopic dipole moment. Upon mechanical compression, the dipole moment density (i.e., polarization) of the fiber mat changes due to the dimensional effect, generating electric charges and voltage with a high direct d₃₃. Similarly, electrically poled porous polymer (e.g., polypropylene) films can also exhibit high piezoelectric coefficient in the range of 200-600 pC/N.[55] However, due to the high compliance of electrospun fiber mats and porous

polymer films, the electromechanical coupling factor is low. Therefore, they are more suitable for electromechanical sensors, rather than actuators and transducers.

Most recently, we reported a viable approach to induce SC_{OAF} in PVDF homopolymers without any ECC structure.[33] After high-power ultrasonication, certain nanosized crystals were broken off from the PC lamella, forming OAF and SC_{OAF}. Consequently, the piezoelectric performance is significantly enhanced via electrostriction of the OAF and relaxor-like SC_{OAF}, and the maximum inverse d₃₁ reached 75 pm/V at 65 °C. However, it is still unclear what controls the OAF and SC_{OAF} formation and whether the piezoelectric performance can be further enhanced or not. We know that PVDF homopolymers contain 3-7 mol.% head-to-head and tail-to-tail (HHTT) defects. In this work, we carry out systematic studies to understand the effect of HHTT chemical defects on the formation of OAF and SC_{OAF} and the subsequent piezoelectric performance of high-power ultrasonicated PVDF films having different HHTT defect contents.

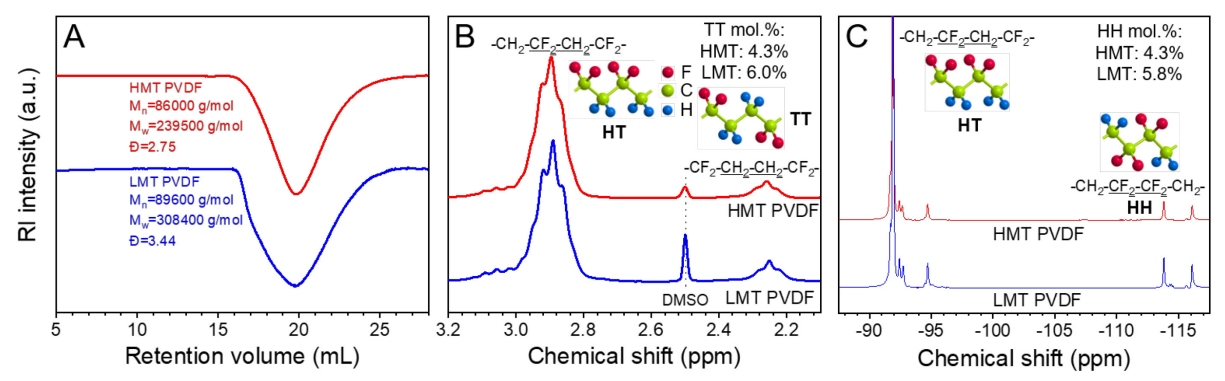


Fig. 1. Molecular characterization for HMT and LMT PVDF samples. (A) SEC results with the DMF flow rate of 1.0 mL/min. (B) 1 H and (C) 19 F NMR spectra in d₆-DMSO.

2. Results and discussions

2.1. Effect of chemical defects and processing conditions on the crystalline structures of high melting temperature (HMT) and low melting temperature (LMT) PVDF films

Two grades of PVDF with different T_ms were used in this study. To understand the origin of different T_ms of these PVDF homopolymers, molecular characterization using SEC and NMR was carried out. As shown in Fig. 1A, the two PVDF samples had a similar number-average molecular weight (M_n) and dispersity index (Đ). For the HMT PVDF, the M_n was 86000 g/mol and the Đ was 2.75. For the LMT PVDF, the M_n and Đ were 89600 g/mol and 3.44, respectively. The slight difference in M_n and Đ would not explain the T_m difference for the HMT and LMT PVDF samples. Then, ¹H and ¹⁹F NMR were used to reveal the chemical defects in the polymer chains (Figs. 1B and C), i.e., head-to-head (HH, the -CH₂-<u>CF₂-CF₂-CH₂-</u> sequence as determined by ¹⁹F NMR) and tail-to-tail (TT, the -CF₂-<u>CH₂-CH₂-CF₂-</u> sequence as determined by ¹H NMR) defects. The chemical structures of the head-to-tail (HT), HH, TT sequences are shown in the insets of Figs. 1B and C. In the ¹H NMR spectra (Fig. 1B), the content of the TT defects was calculated by integrating the peaks centered at 2.3 and 2.9 ppm, using the following equation:

$$HH(TT)\% = \frac{0.25A_{HH(TT)}}{0.5A_{HT} + 0.25A_{HH(TT)}} \times 100\%$$
 (1)

In 19 F NMR, A_{HH} is the integrated area from -113.3 to -116.7 ppm, A_{HT} is the integrated area from -90.5 to -95.5 ppm. In 1 H NMR, A_{TT} is the integrated area from 2.1 to 2.3 ppm, and A_{HT} is the integrated area from 2.8 to 3.2 ppm. The HMT PVDF had a lower TT% of 4.3% than the LMT PVDF (TT% = 6.0%). Using Eqn. (1), the HH% was also calculated: 4.3% for the HMT PVDF and 5.8% for the LMT PVDF. For a long chain polymer, TT% should be equal to HH%. The slight difference in the TT% and HH% for the LMT PVDF could come from experimental error. During

crystallization, the HHTT defects must be excluded from the crystalline lamellae, possibly accumulated in the OAF, which linked between the crystalline lamellae and the IAF. The different HHTT contents of these two PVDF samples should originate from different polymerization conditions. It is known that most commercial PVDF resins are polymerized via either suspension or emulsion polymerization.[56] Usually, a lower temperature in suspension polymerization leads to a lower HHTT content. Therefore, we infer that the HMT PVDF should be suspension polymerized at a lower temperature than the LMT PVDF.

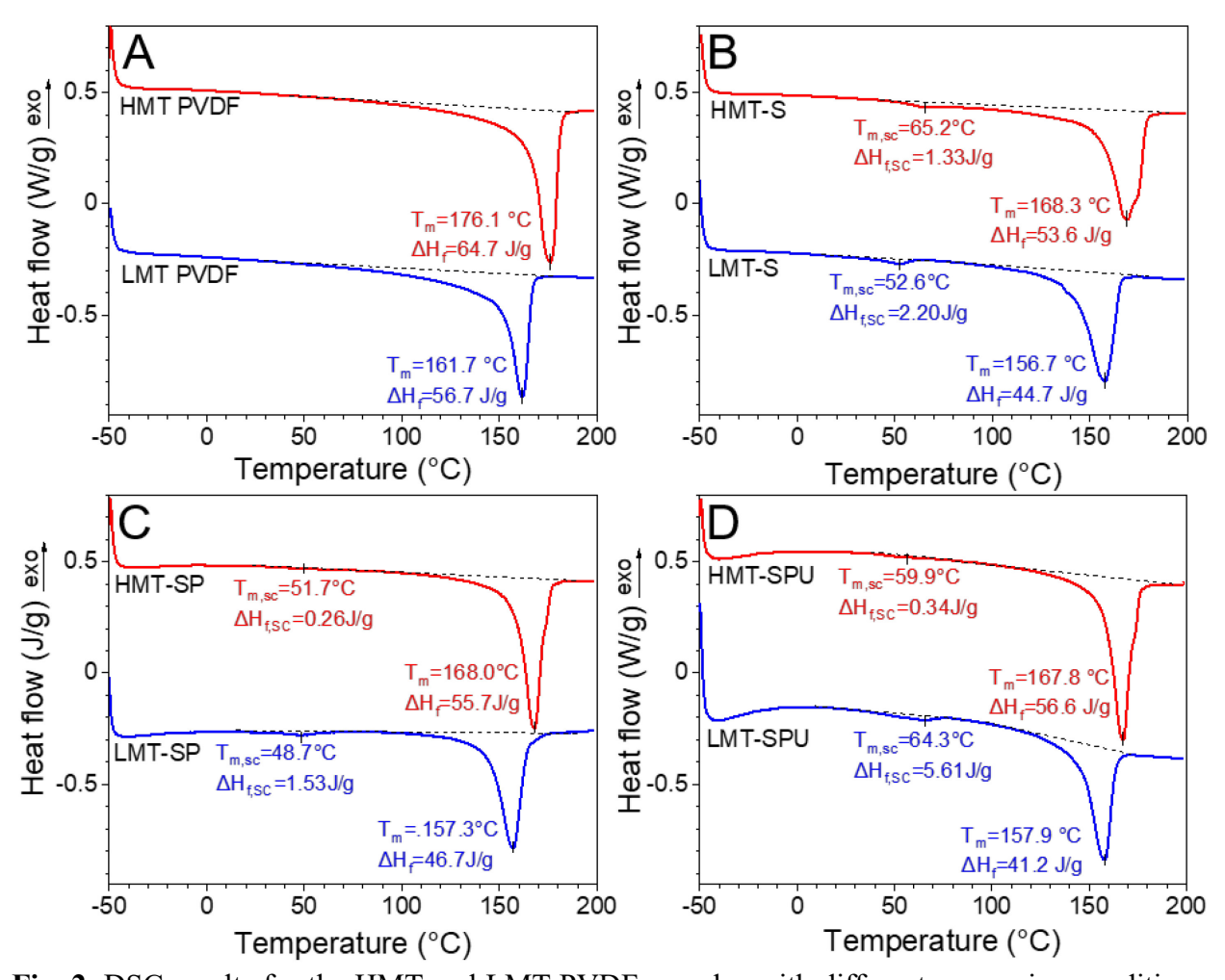


Fig. 2. DSC results for the HMT and LMT PVDF samples with different processing conditions:

(A) Second heating curve after removing the prior thermal history, (B) uniaxially stretched (S) samples, (C) uniaxially stretched and poled (SP) samples, and (D) uniaxially stretched, poled, and ultrasonicated (SPU) samples.

It must be the different HHTT contents that caused the different T_ms for the HMT and LMT PVDF samples, as examined by DSC measurements. Fig. 2A shows the DSC curves during the second heating at 10 °C/min after cooling from the melt at the same rate. Using this method, the prior thermal history was removed, and the T_m s of the primary crystals (T_m^{PC}) were determined. The HMT PVDF had a higher T_m^{PC} of 176.1 °C than the LMT PVDF (161.7 °C). Moreover, the HHTT defects are expected to affect the crystalline structure during film processing. For the stretched (S), stretched and poled (SP), and stretched, poled, and ultrasonicated (SPU) PVDF samples, other than T_m^{PC} , a weak melting peak of the secondary crystals (T_m^{SC}) was observed at 48-65 °C. By integrating the melting peaks of the primary and secondary crystals in Figs. 2B-D, their heats of fusion (ΔH_f^{PC} and ΔH_f^{SC}) were also determined. Results of T_m^{PC} , T_m^{SC} , ΔH_f^{PC} , and ΔH_f^{SC} for both HMT and LMT PVDF samples with S, SP, and SPU processing conditions are summarized in Table 1. For primary crystals, the T_m^{PC} differences between HMT and LMT PVDF samples were as large as 10-12 °C. However, the T_m^{PC} differences for the S, SP, and SPU samples within the same PVDF group, either HMT or LMT, were no greater than 1.2 °C.

Table 1. Summary of the DSC, SAXS, and WAXD results for different PVDF samples.

	HMT-S	HMT-SP	HMT-SPU	LMT-S	LMT-SP	LMT-SPU
T_m^{PC} (°C)	168.3	168.0	167.8	156.7	157.3	157.9
ΔH_f^{PC} (J/g)	53.6	55.7	56.6	44.7	46.7	41.2
T_m^{SC} (°C)	65.2	51.7	59.9	52.6	48.7	64.3
ΔH_f^{SC} (°C)	1.33	0.26	0.34	2.20	1.53	5.61

L (nm)	9.77	9.83	9.75	5.98	6.31	6.04
$oldsymbol{x}_{ ext{c}}$	0.434	0.524	0.515	0.375	0.408	0.400
$\boldsymbol{x}_{ ext{OAF+SC}}$	0.264	0.249	0.260	0.323	0.317	0.326
$oldsymbol{x}_{ ext{IAF}}$	0.301	0.227	0.225	0.302	0.275	0.274

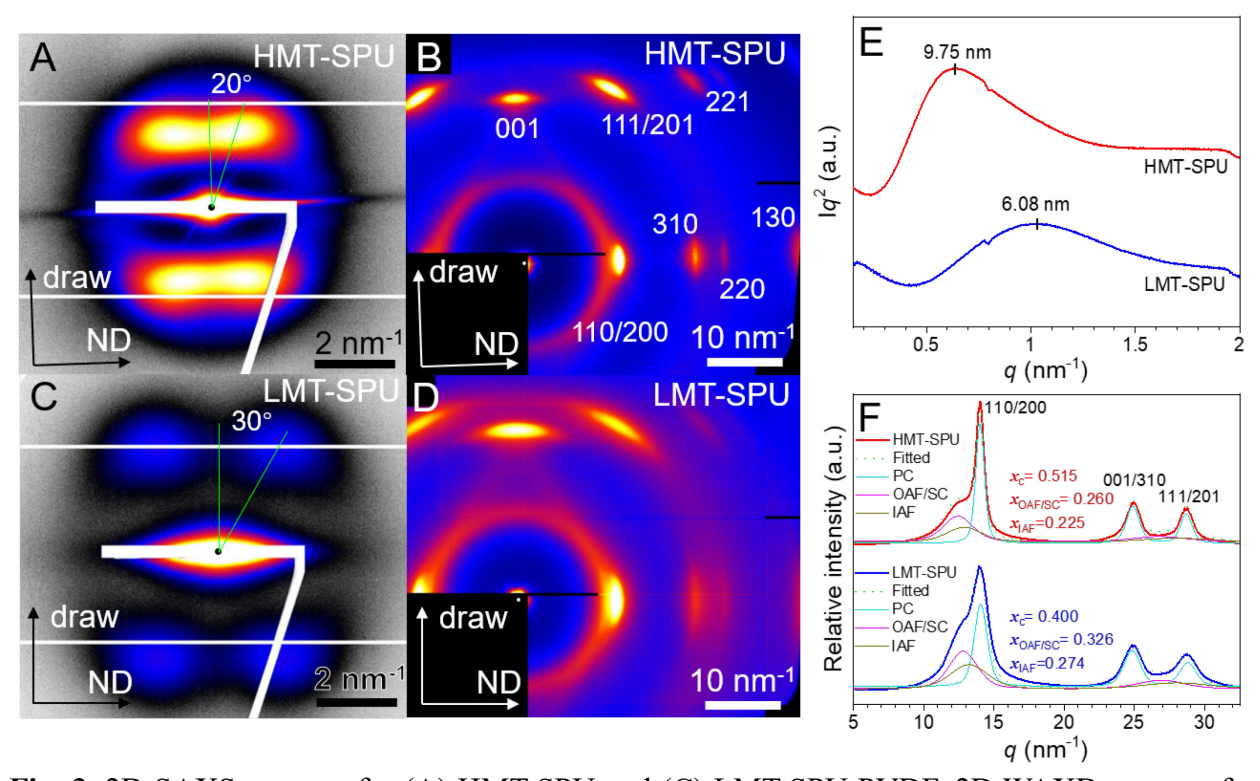


Fig. 3. 2D SAXS patterns for (A) HMT-SPU and (C) LMT-SPU PVDF. 2D WAXD patterns for (B) HMT-SPU and (D) LMT-SPU PVDF. The uniaxial stretching direction is in the vertical direction. The X-ray intensity in the 2D SAXS and WAXD images is in a logarithmic scale. (E) 1D SAXS results from (A) and (C). (F) 1D WAXD results from (B) and (D). Peak deconvolution is performed using the Peakfit software for the PC, OAF/SC, and IAF, following previous reports.[31]

The complex crystalline structures in these PVDF samples were investigated by synchrotron small-angle X-ray scattering (SAXS) and wide-angle X-ray diffraction (WAXD). Fig. 3 show the 2D SAXS and WAXD results for the HMT-SPU and the LMT-SPU PVDF films. For other S and SP PVDF films, the SAXS and WAXD results are presented in Figs. S1 (2D patterns) and S2 (1D curves) in the Supporting Information. From the 2D SAXS results, a butterfly pattern was seen, suggesting lamella-tilting with respect to the drawing direction, i.e., 70° for the HMT-

SPU PVDF and 60° for the LMT-SPU (Figs. 3A and C). Fig. 3E shows the 1D Lorentz-corrected SAXS curves for the HMT-SPU and the LMT-SPU samples. Using the correlation function analysis of the SasView software, the overall lamellar spacings were determined to be 9.75 and 6.08 nm for the HMT-SPU and the LMT-SPU PVDF, respectively. We consider that the higher content of HHTT defects in the OAF of the LMT-SPU PVDF caused a higher lamella-tilting angle and thinner crystalline lamellar thickness than the HMT-SPU PVDF. Similar results were also seen for other S and SP samples (Fig. S1).

For the stretched HMT-S film, a small fraction of α crystals remained in the sample (Fig. S1B). After high-field electric poling at 400 MV/m, the remaining α crystals largely disappeared (Fig. S1G). For the LMT-S and the LMT-SP films, no α crystal reflections were seen in Figs. S1D and H. After high-power ultrasonication, both HMT-SPU and LMT-SPU samples exhibited oriented β crystal reflections: $(110/200)_{\beta}$ on the equator, $(001)_{\beta}$ on the meridian, and $(111/201)_{\beta}$ in the quadrant (Figs. 3B,D). However, the two WAXD patterns in Figs. 3B and D looked different because the sharp (001)_B and (111/201)_B reflections of the LMT-SPU PVDF were surrounded by more diffuse scattering than those for the LMT-SPU PVDF. The sharp reflections were attributed to the diffraction from PCs with long-range order, and the diffuse scattering around the sharp reflections should originate from the OAF and SCs with a poor crystal structure. Using the Peakfit software, the integrated 1D WAXD curves were deconvoluted into 3 components: PCs (x_c) , OAF+SCs ($x_{OAF/SC}$), and IAF (x_{IAF}), following the method used in our recent reports.[31] The results for the HMT-SPU and the LMT-SPU samples are shown in Fig. 3F. The HMT-SPU sample exhibited a significantly higher primary crystallinity ($x_c = 0.515$) than the LMT-SPU sample ($x_c =$ 0.400), whereas the LMT-SPU sample had a higher $x_{IAF} = 0.274$ than the HMT-SPU sample (x_{IAF} = 0.225). Meanwhile, the LMT-SPU sample had a higher $x_{OAF/SC}$ of 0.326 than the HMT-SPU

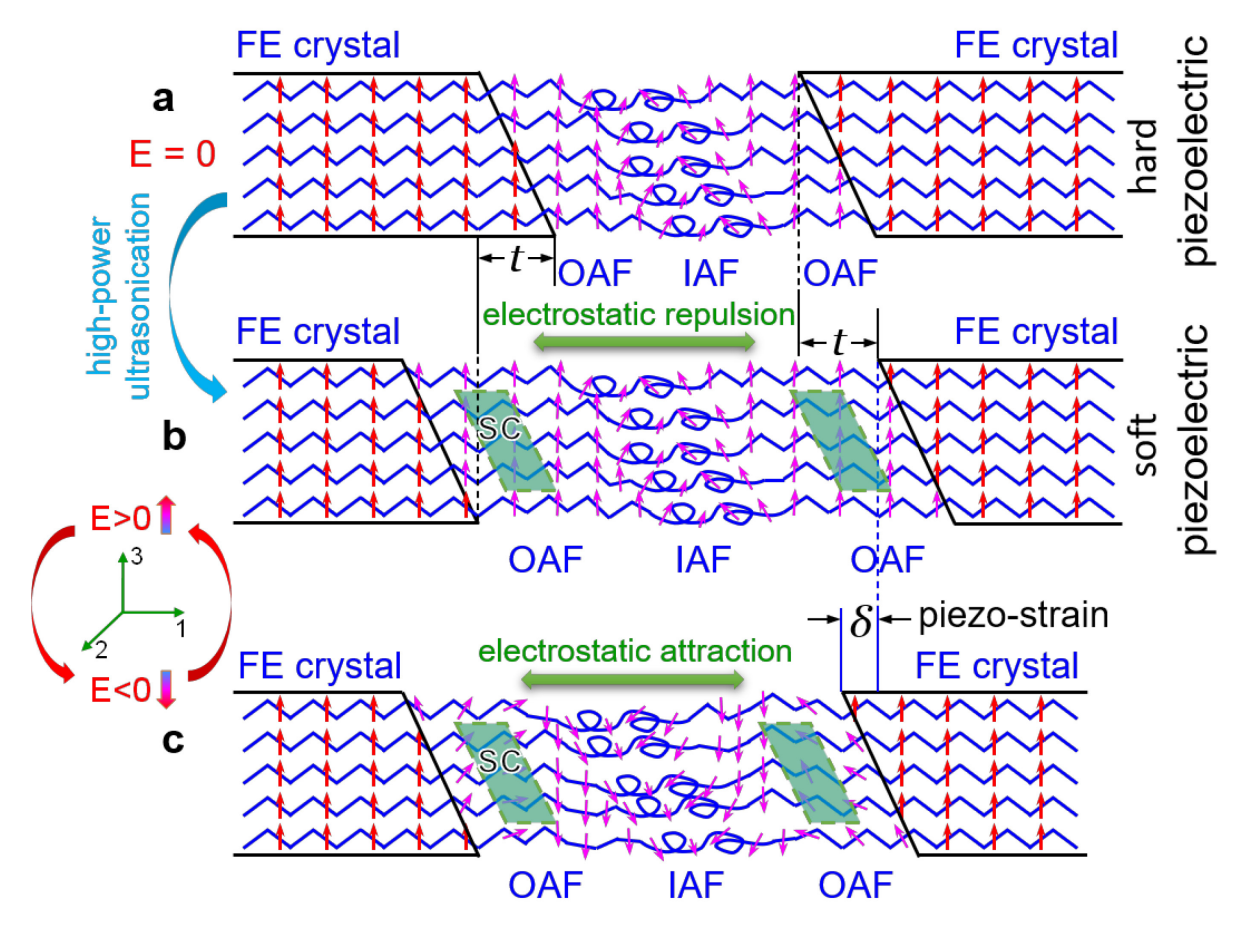
($x_{OAF/SC} = 0.260$). Combining the results from SAXS and WAXD, the effect of the HHTT defects could be identified. Namely, the HHTT defects decreased the crystalline lamellar thickness and x_c , and increased $x_{OAF/SC}$ and x_{IAF} . During crystallization, the PVDF chains with a higher HHTT content were expelled from the PC lamellae, forming the OAF (and the IAF as well). As a result, the crystalline lamellae became thinner with a lower x_c . The 1D WAXD curve deconvolution results for other HMT and LMT samples are presented in Fig. S3-S5, and the x_c , $x_{OAF/SC}$, and x_{IAF} data are summarized in Table 1.

In addition to different HHTT contents between HMT and LMT PVDF, processing conditions also affected the semicrystalline structures. First, both stretched HMT and LMT samples showed an increase of the ΔH_f^{PC} after electric poling and then a decrease after high-power ultrasonication (Table 1). The former effect could be attributed to the increased primary crystallinity x_c from mechanical stretching. The latter effect was attributed to the tendency of high-power ultrasonication to break some SCs off from the PC lamellae, as we reported recently.[33] This is reflected by the increased ΔH_f^{SC} for the SPU samples compared to the SP samples. However, such an effect was quite different for the HMT and LMT PVDF samples. Compared to the SP samples, the LMT-SPU sample had a large change of ΔH_f^{SC} from 1.53 to 5.61 J/g (4.08 J/g difference), but the ΔH_f^{SC} of the HMT-SPU sample only increased from 0.26 to 0.34 J/g (0.08 J/g difference). Second, the WAXD analysis of these samples also exhibited a similar trend for the x_{OAF+SC} . Basically, after electric poling, the x_{OAF+SC} decreased slightly for the SP samples, as compared to the S samples. However, it returned to the same levels for the SPU samples after high-power ultrasonication (Table 1).

During the review process, some questions were raised regarding the ultrasonication effect.

The first question was the neat ultrasonication effect without stretching and electric poling. As we

know, without electric poling, the ferroelectric samples will not show any piezoelectricity. Therefore, we used DSC to demonstrate the neat ultrasonication effect, using LMT PVDF samples as an example. As sown in Fig. S6A, the ΔH_f^{SC} was obtained by integrating the peak around $T_m = 45-60$ °C. Comparing LMT-QU with LMT-Q, the ΔH_f^{SC} increased from 1.86 J/g to 3.90 J/g. Comparing LMT-S with LMT-SU, the ΔH_f^{SC} increased from 2.31 J/g to 3.77 J/g. Obviously, ultrasonication by itself would break some SCs off from the PCs, together with the OAF, which happened even independent of stretching and/or electric poling. The second question was the ultrasonication effect studied by Fourier transform infrared (FTIR) spectroscopy. As shown in Fig. S6B, no obvious difference could be identified after ultrasonication of both HMT-SP and LMT-SP samples. This is largely attributed to the low content for SCs, which is less than 5%. With such a low content and due to their disordered structures, it is very difficult to see clear changes after ultrasonication using FTIR. Similar situation is also observed for WAXD (see Fig. S2B).



Scheme 1. Schematic representations of the formation mechanism of OAF and SC_{OAF} by high-power ultrasonication and the inverse piezoelectricity in PVDF with β crystals. (a) The SP sample at E=0 and the SPU sample at (b) E>0 and (c) E<0. Red and magenta arrows are the VDF dipoles in the poled β crystals and the amorphous phase (OAF + IAF), respectively. The green parallelograms in the OAF are SC_{OAF} . Reproduced by permission from ref. [33]. Copyright Royal Society of Chemistry 2022.

From the above structural studies, the effect of high-power ultrasonication on the semicrystalline morphology change can be understood via the schematic representation in Schemes 1a,b. First, the SP sample contains a certain amount of OAF linking between the PC lamellae and the IAF. Then, upon ultrasonication, certain crystals in the surface layers are broken off from the PC lamellae, forming OAF and SC_{OAF}. This is why the primary crystallinity x_c slightly decreases and the secondary crystallinity increases after ultrasonication. The SC_{OAF} must have a poor crystalline structure and became relaxor-like. Although the x_{OAF+SC} variation was only about

0.01, we expect that this small difference in the semicrystalline structures will significantly influence the dielectric and piezoelectric properties of HMT and LMT PVDF films, because it has been reported that the crystalline-amorphous interfaces play an important role in the piezoelectricity of ferroelectric polymers. [28, 29, 31, 33]

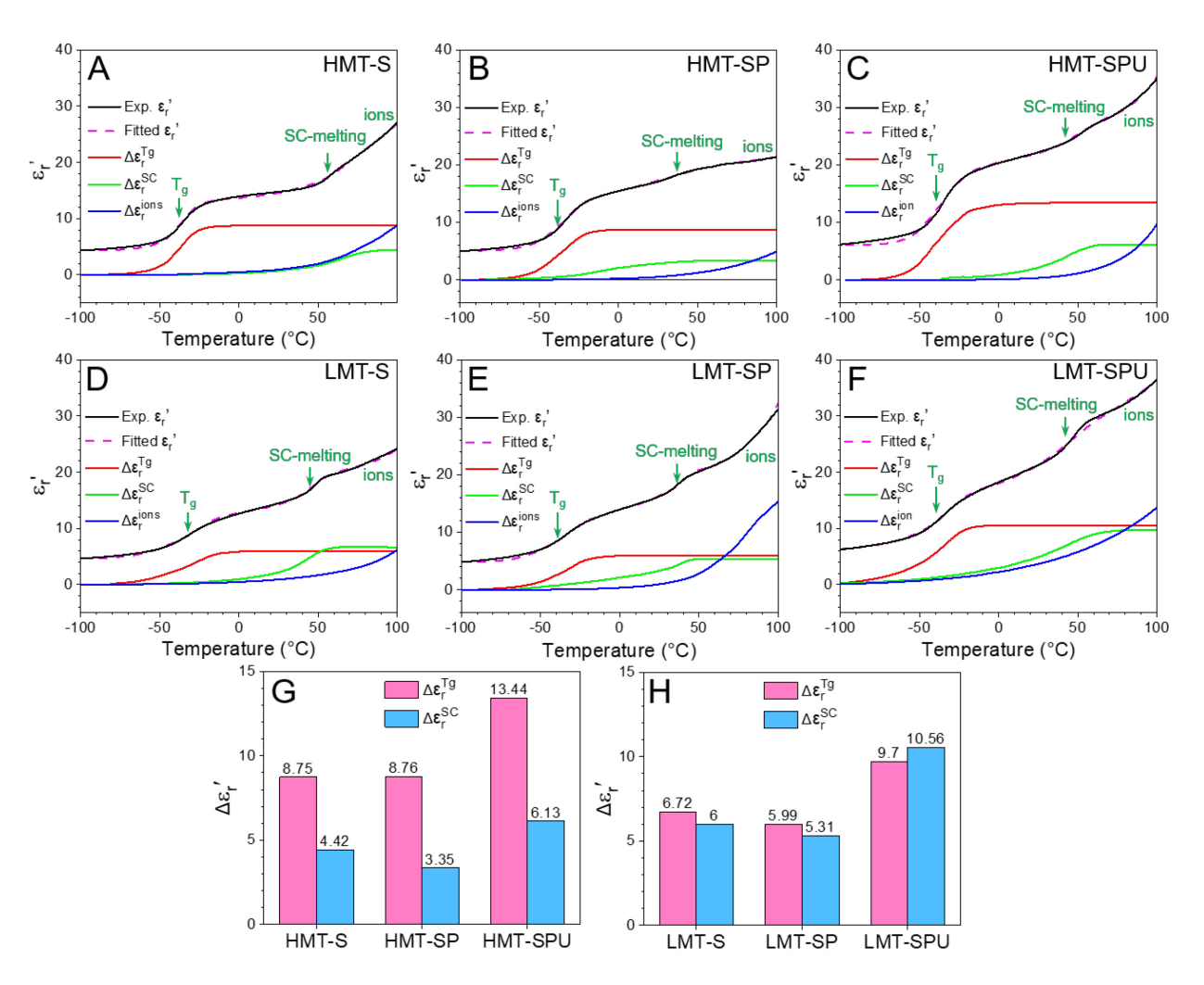


Fig. 4. Temperature-scan BDS results of the real part of the relative permittivity (ε_r ') at 1 Hz for (A) HMT-S, (B) HMT-SP, (C) HMT-SPU, (D) LMT-S, (E) LMT-SP, and (F) LMT-SPU PVDF films. The heating rate was 2 °C/min. Following our previous report,[33] the ε_r ' curves are deconvoluted into the $\Delta \varepsilon_r^{Tg}$, $\Delta \varepsilon_r^{SC}$ and $\Delta \varepsilon_r^{ion}$ components, which are summarized in (E) and (F) for various HMT and LMT PVDF, respectively.

2.2. Linear dielectric property of various HMT and LMT PVDF films

The linear dielectric property was studied by BDS at a low AC electric field (~0.1 MV/m with frequency being 1 Hz to 1 MHz) in a temperature range of -100 to 155 °C: Fig. S7 for the HMT samples and Fig. S8 for the LMT samples. In this temperature range, three dielectric relaxation events were identified for the real part (ε_{r}') and the imaginary part (ε_{r}'') of the relative permittivity during heating (1 Hz): glass transition at -40 °C, melting of SC at ca. 60 °C, and impurity ionic conduction starting around 75 °C. Note, even though the impurity ion concentration in PVDF is less than 1 ppm, the thermally activated conduction of fast ions (e.g., Na⁺) can cause significant interfacial polarization (i.e., both ε_r' and ε_r'' increases at low frequencies and high temperatures), when the temperature is higher than 75 °C.[57-59] For both HMT and LMT samples, the ε_r' slightly decreased after electric poling and then increased after ultrasonication. To quantify these changes, we performed deconvolution of ε_{r}' (and ε_{r}'') curves in Figs. 4A-F into separate contributions from the glass transition ($\Delta \varepsilon_r^{Tg}$, T_g is the glass transition temperature), melting of SCs ($\Delta \varepsilon_r^{SC}$), and impurity ion conduction ($\Delta \varepsilon_r^{ion}$), following our recent reports.[33, 58, 59] The multimode Havriliak-Negami (HN) formula was used for the deconvolution. Figs. 4A-F show the deconvolution results for various HMT and LMT samples, and the fitted $\Delta \varepsilon_r^{Tg}$, $\Delta \varepsilon_r^{SC}$ and $\Delta \varepsilon_r^{ion}$ values are shown in Fig. 4G for the HMT samples and Fig. 4H for the LMT samples. Comparison of the S and SP samples for both LMT and HMT PVDF showed that the $\,\Delta arepsilon_r^{Tg}\,$ did not change much after electric poling. However, the $\Delta \varepsilon_r^{SC}$ slightly decreased, i.e., 1.07 for the HMT-SP and 0.69 for the LMT-SP sample. After ultrasonication, both HMT-SPU and LMT-SPU showed substantial increases in ε_r '. For the HMT-SPU PVDF, $\Delta \varepsilon_r^{Tg}$ increased 4.68 and $\Delta \varepsilon_r^{SC}$ increased 2.78 compared to the HMT-SP PVDF, suggesting that the increase in $\varepsilon_{\rm r}'$ of HMT-SPU

primarily came from the orientational polarization of the OAF. On the other hand, the LMT-SPU sample had a $\Delta \varepsilon_r^{Tg}$ increase of 3.71 and a $\Delta \varepsilon_r^{SC}$ increase of 5.25, indicating that the increase in ε_r' of LMT-SPU primarily came from the orientational polarization of the relaxor-like SC_{OAF}. Since the piezoelectric constant is proportional to the dielectric constant (see Eqn. 4), we expect that the LMT-SPU sample should have a higher piezoelectric performance than the HMT-PUT sample.

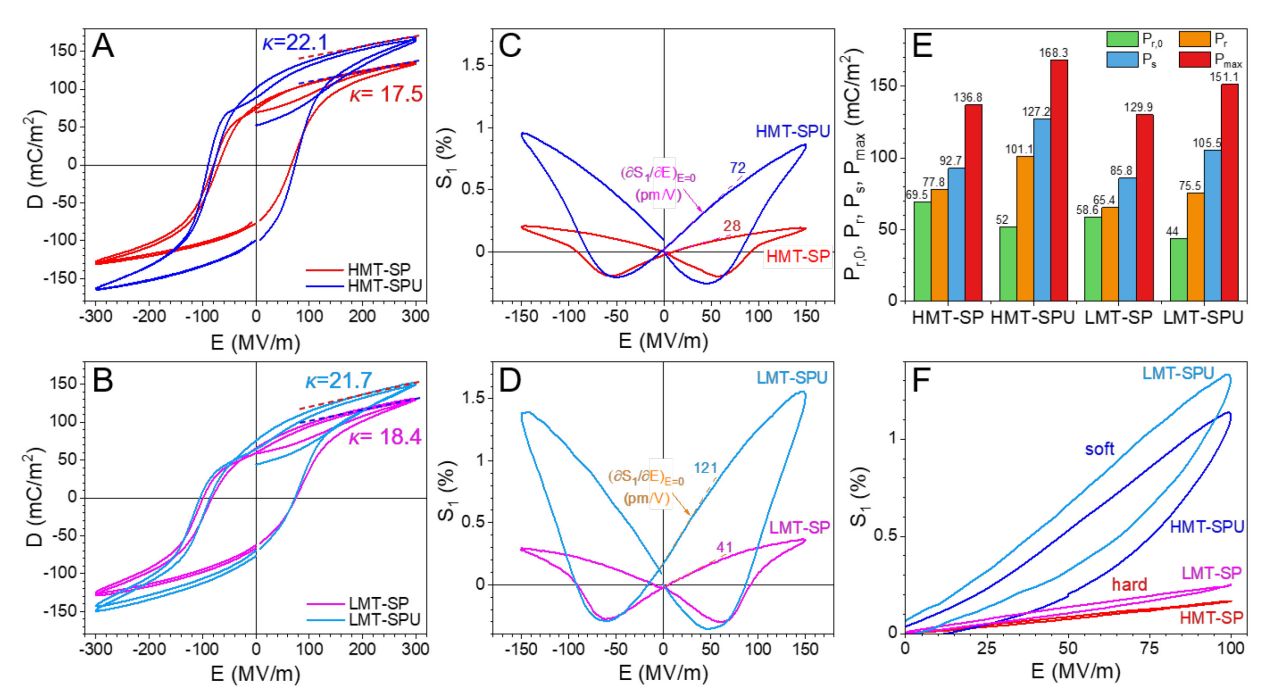


Fig. 5. Bipolar D-E loops for (A) HMT-SP and HMT-SPU PVDF, and (B) LMT-SP and LMT-SPU PVDF. Bipolar S_1 -E loops for (C) HMT-SP and HMT-SPU PVDF, and (D) LMT-SP and LMT-SPU PVDF. (E) $P_{r,0}$, P_r , P_s , and P_{max} values for the HMT and LMT PVDF films obtained from (A) and (B). (F) Unipolar S_1 -E loops of the HMT and LMT PVDF films.

2.3. Ferroelectric properties of various HMT and LMT PVDF films

The ferroelectric properties for the HMT and LMT SP samples with and without ultrasonication were studied by bipolar D-E and S₁-E loops.[60, 61] Figs. 5A and B show bipolar D-E loops at 300 MV/m for HMT and LMT SP and SPU samples, respectively. The P_{r,0}, P_r, P_s and P_{max} values during bipolar poling were determined and summarized in Fig. 5E, following our

previous report.[30] After ultrasonication, both HMT and LMT SPU samples showed decreased P_{r0} . For example, it dropped from 69.5 mC/m² for the HMT-SP PVDF to 52.0 mC/m² for the HMT-SPU PVDF. For the LMT samples, it decreased from 58.6 mC/m² for the LMT-SP PVDF to 44.0 mC/m² for the LMT-SPU PVDF. The decrease of $P_{r,0}$ was consistent with the reduced content of poled PCs and the increased content of the mobile OAF and relaxor-like SC_{OAF} after ultrasonication. Meanwhile, P_r , P_s , and P_{max} increased after high-power ultrasonication, indicating enhanced polarizability due to the increased OAF and SC_{OAF} in the SPU samples. Especially for the HMT-SPU sample, the P_s achieved a value as high as 127.2 mC/m², which is comparable to the highest reported P_s of a poled BOPVDF film with 100% β crystals, i.e., 140 mC/m².[10, 30] In addition, the apparent dielectric constants (κ) were determined from the slope of the deformational polarization at high fields. After ultrasonication, both HMT-SPU and LMT-SPU showed an increased κ : from 17.5 for HMT-SP to 22.1 for HMT-SPU, and from 18.4 for LMT-SP to 21.7 for LMT-SPU. This is consistent with the above BDS results of increased permittivity after ultrasonication for the HMT-SPU and the LMT-SPU samples.

Comparing HMT and LMT samples, the LMT-SP and SPU samples exhibited less pronounced ferroelectricity with lower P_r , P_s , and P_{max} values (see Figs. 5A, B, and E). This is because more HHTT defects in the LMT PVDF prevented the growth of larger ferroelectric domains during high-field poling. However, the high-field electro-actuation of the LMT SP and SPU samples was greater than that of the HMT SP and SPU samples, and this can be seen from the bipolar S_1 -E loops at 150 MV/m in Figs. 5C and D. In addition, the slope during the depolarization loop, $(\partial S_1/\partial E)_{E=0}$, was considered to be closely related to piezoelectricity as discussed in previous reports.[29, 31] The SPU samples after ultrasonication showed enhanced $(\partial S_1/\partial E)_{E=0}$ compared to the SP samples. We therefore expect that the LMT samples should exhibit

higher piezoelectric performance than the HMT samples. Fig. 5F shows the in-situ high-field unipolar S_1 -E loop at 100 MV/m. Two SP samples exhibited a linear response with low actuation, while two SPU samples had significantly enhanced S_1 with a large hysteresis. For piezoelectric ceramics, a similar hard-to-soft transition is also observed.[18, 62] A piezoelectric ceramic with a linear electro-actuation is called a hard piezoelectric, while that with nonlinear electro-actuation is called a soft piezoelectric. The soft-to-hard piezoelectric transition is usually realized by chemically doping the hard piezoelectric with a heavier element to enhance the domain wall motion.[18, 62] Such a transition, however, has never been achieved for piezoelectric polymers before. We expect that the polymers with a "hard-to-soft" piezoelectric transition will exhibit better piezoelectric performance due to enhanced electrostriction from both OAF and relaxor-like SC_{OAF} .

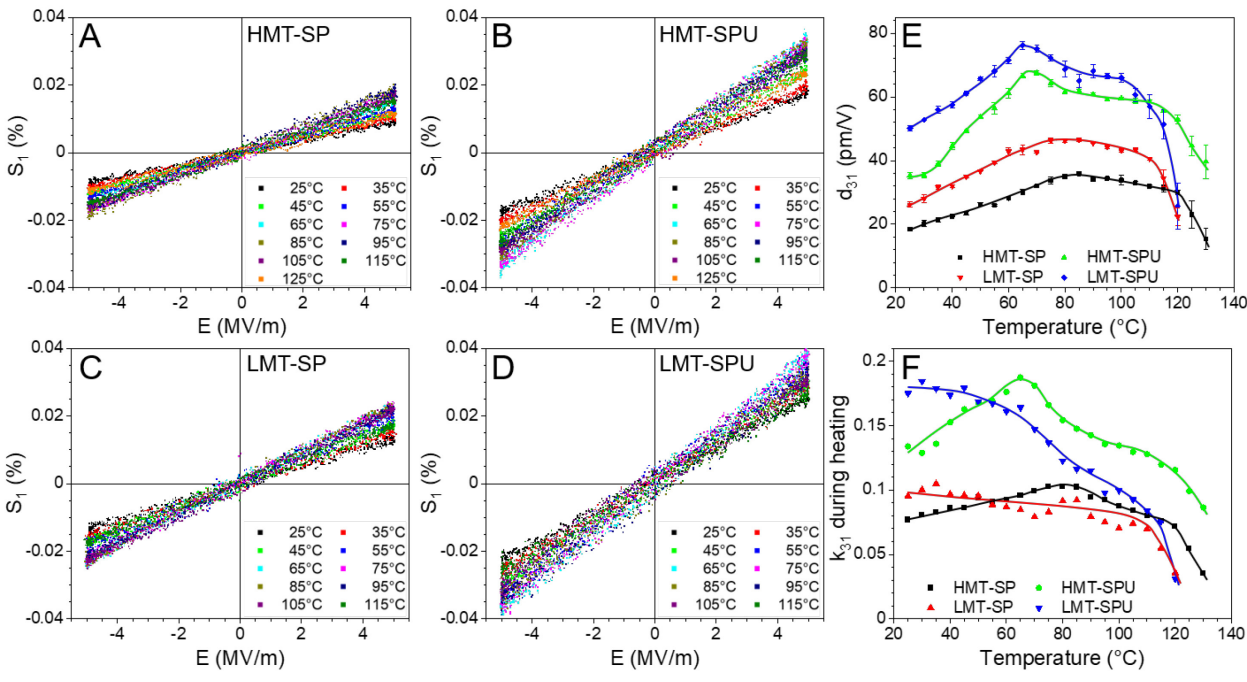


Fig. 6. Low-field S₁-E loops for (A) HMT-SP, (B) HMT-SPU, (C) LMT-SP, and (D) LMT-SPU at different temperatures. Calculated (E) inverse d₃₁ and (F) k₃₁ for the samples in (A-D).

2.4. Inverse piezoelectric properties of various PVDF films for actuation

The inverse piezoelectricity of the HMT and LMT SP and SPU samples was measured

using bipolar S₁-E loops at a low field of 5 MV/m, as shown in Figs. 6A-D and Figs. S9. The inverse d_{31} was obtained from the equation: $S_1 = d_{31} \cdot E$, where S_1 is the strain in the stretching direction and E is the electrical field. As shown in Fig. S10, the S₁-E loops before and after shorting both electrodes on the film surfaces are identical. This result indicates that the surface electrostatic charges, which are generated by sample-handling, are negligible for the piezoelectric property measurement. At room temperature, the HMT-SP and LMT-SP showed typical inverse d₃₁ values for PVDF, i.e., 18.4±0.6 and 26.2±0.9 pm/V, respectively. After ultrasonication, the SPU samples exhibited enhanced inverse d₃₁ values, i.e., 35.3±0.9 pm/V for HMT-SPU and 50.2±0.8 pm/V for LMT-SPU. Upon heating to 70 °C, four PVDF samples showed increased d₃₁ with increasing temperature. For the SPU samples, the maximum points were reached around 65-70 °C, and the highest inverse d_{31} values were 66.6 ± 0.7 pm/V for the HMT-SPU and 76.2 ± 1.2 pm/V for the LMT-SPU, respectively. Note, these highest d_{31} temperatures corresponded well to the T_m^{SC} , and it is likely that the relaxor-like SC_{OAF} enhanced the piezoelectric performance. For the SP samples, the enhancement of d₃₁ upon heating was relatively weak, no greater than 20 pm/V for both HMT and LMT. Meanwhile, the electromechanical coupling factor k_{31} was calculated using the equation: $k_{31} = d_{31}(Y_1/\epsilon_r\epsilon_0)^{0.5}$, where Y_1 was the Young's modulus in the stretching direction. The Y_1 values of the HMT and LMT SP and SPU samples were obtained from the stress-strain curves at different temperatures, as shown in Fig. S11. Among all samples, the HMT-SPU PVDF showed the highest k₃₁ of 0.187 at 65 °C, primarily due to its higher Young's modulus. From the inverse d₃₁ and k₃₁ results, the upper limits of d₃₁ thermal stability could be determined, i.e., 110 °C for LMT SP and SPU samples and 120 °C for HMT SP and SPU samples. Above these temperatures, both d₃₁ and k₃₁ started to decrease.

The enhanced inverse piezoelectricity can be understood via the schematic representation

in Scheme 1b,c. When a positive electric field is applied, the mobile dipoles in the OAF and SC_{OAF} are aligned upward, which is in the same direction as the poled β crystals nearby. Consequently, electrostatic repulsion will push the neighboring β crystals apart, resulting in elongation in the 1 (stretching) direction (and also shrinkage in the 3 direction). When a negative electric field is applied, the mobile dipoles in the OAF and SC_{OAF} are aligned downward, which is in the opposite direction to the poled β crystals nearby. Electrostatic attraction will shrink the sample along the 1 (stretching) direction (and also thickening it in the 3 direction). We speculate that the ultrasonication-induced SC_{OAF} should have a poor crystalline structure and thus be relaxor-like; therefore, the inverse piezoelectricity is expected to be significantly enhanced by the high-power ultrasonication via the SC_{OAF}. Note that the maximum inverse d₃₁ around 65 °C could not be explained by the pyroelectricity of PVDF, because it decreases the polarization with increasing temperature up to 120 °C and the pyroelectric coefficient remains constant. [63] Above 85 °C, the inverse d₃₁ values of both SPU samples start to decrease and the pyroelectric effect may play some minor role. Above 120 °C, the inverse d₃₁ values decrease to zero and they have nothing to do with the pyroelectric effect.

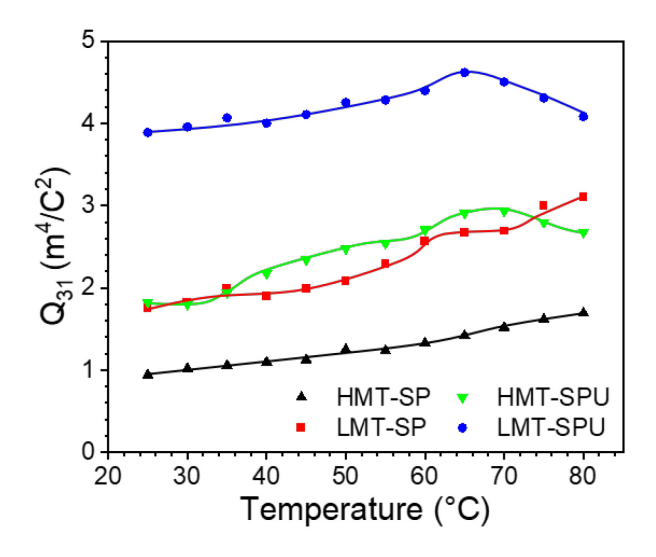


Fig. 7. Calculated electrostriction coefficient Q₃₁ during the first heating process for HMT-SP, HMT-SPU, LMT-SP, and LMT-SPU PVDF films.

According to Eqn. (4), electrostriction coefficient Q_{31} for various HMT and LMT PVDF films can be calculated using the P_{r0} , the d_{31} (Fig. 6E), and the dielectric constant at 1 Hz (Fig. 4). Here, we assume the P_{r0} values stayed almost constant for various HMT and LMT SP and SPU films, when the temperature was below 80 °C.[30] For the dielectric constant, the ionic contribution to $\varepsilon_{r'}$ was subtracted. The temperature-dependent Q_{31} results for various HMT and LMT SP and SPU films are shown in Fig. 7. As we can see, the SPU films exhibited higher Q_{31} values than the SP films. Among all films, the LMT-SPU PVDF films had the highest Q_{31} with values between 4 and 4.6 m⁴/C². This range is typical for electrostrictive PVDF polymers.[15] From these results, we conclude that the electrostriction under a bias polarization (i.e., P_{r0}) was the fundamental reason for the enhanced piezoelectricity.

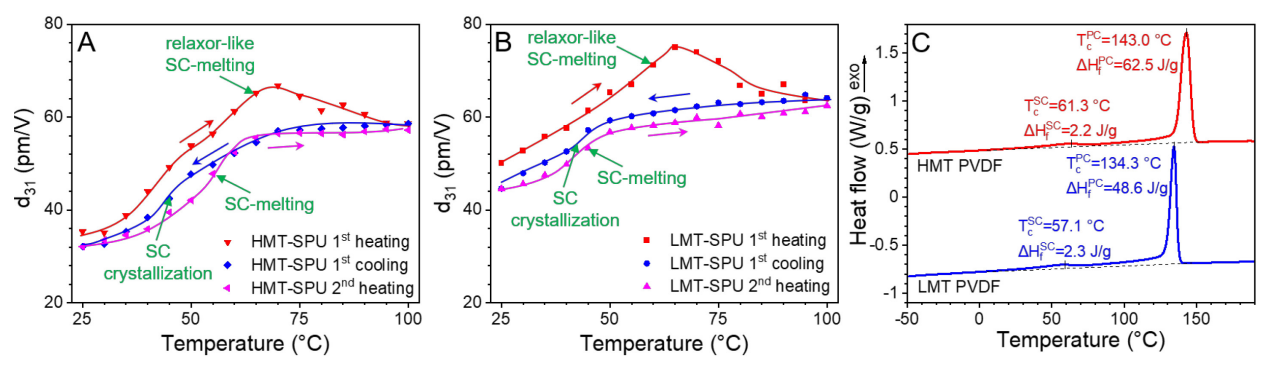


Fig. 8. Inverse d₃₁ during the first heating, the first cooling, and the second heating processes for (A) HMT-SPU and (B) LMT-SPU PVDF films. (C) Cooling DSC curves (10 °C/min) for the HMT-SPU and the LMT-SPU PVDF films.

The thermal reversibility and stability of the piezoelectricity were given by the low-field S₁-E loops during a heating and cooling cycle. Figs. 8A and B show the inverse d₃₁ for the HMT-SPU and the LMT-SPU samples during the first heating, the first cooling, and the second heating

processes. During the first heating, the highest d_{31} points were achieved around the melting of the relaxor-like SC_{OAF} generated by high-power ultrasonication. After the T_m^{SC} , the d_{31} slightly decreased but still kept high, owing to the fact that the relaxor-like SC_{OAF} melted into the mobile OAF. Following the first heating, the first cooling and second heating showed higher d_{31} values than those during the first heating for the SP samples (see Fig. 6E). Meanwhile, the inverse d_{31} of the LMT-SPU sample was higher than that of the HMT-SPU sample. Intriguingly, during the first cooling and second heating, a step change was seen around 50-75 °C. This could be attributed to the crystallization of new SCs in the OAF during the first cooling and their subsequent melting upon the second heating. The formation of new SC_{OAF} was confirmed by the DSC cooling curves shown in Fig. 8C for HMT and LMT PVDF samples: the SC_{OAF} crystallization was seen at 61.3 °C ($\Delta H_f^{SC} = 2.2 \text{ J/g}$) for HMT PVDF and 57.1 °C ($\Delta H_f^{SC} = 2.3 \text{ J/g}$) for LMT PVDF. However, the new SC_{OAF} from melt-recrystallization was less polarizable than the SC_{OAF} generated by the high-power ultrasonication.

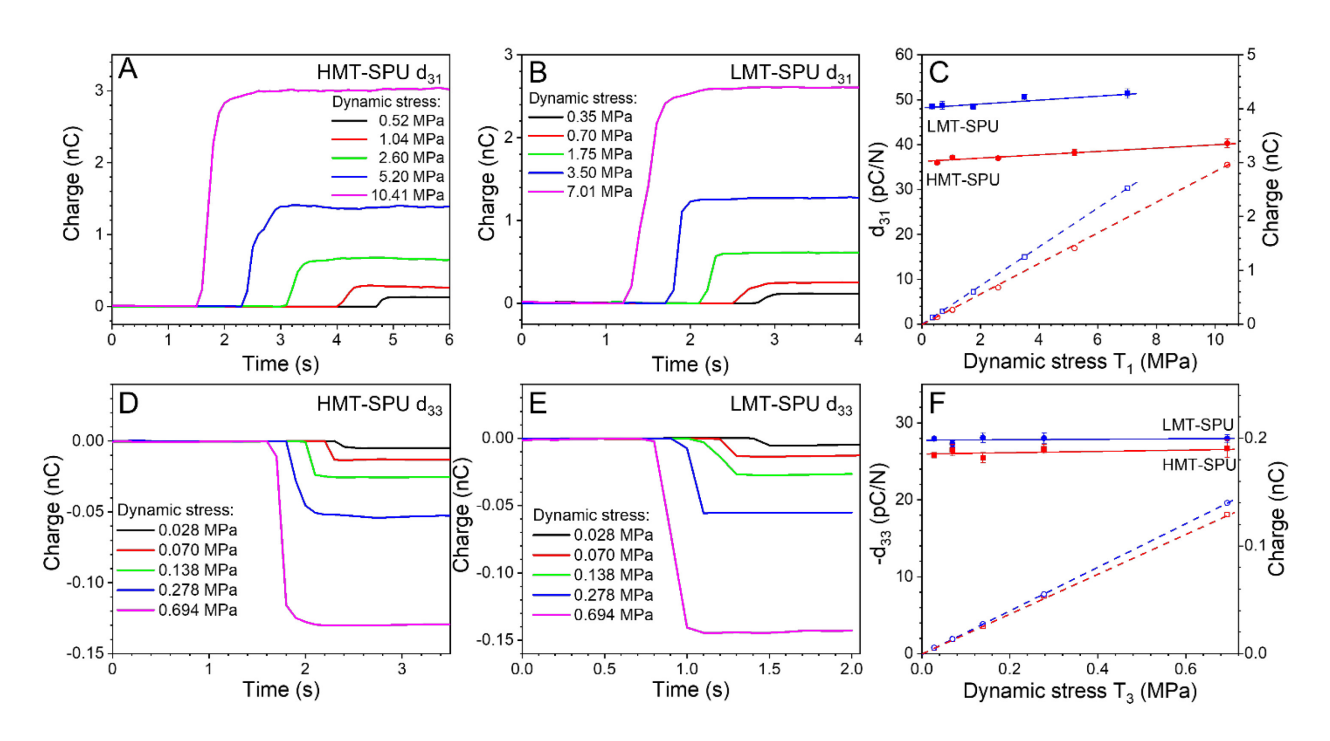


Fig. 9. Direct piezoelectric charge generation during (A,B) tensile stress (T_1) for (A) HMT-SPU and (B) LMT-SPU films and (D,E) compression stress (T_3) for (D) HMT-SPU and (E) LMT-SPU films. (C) and (D) show the charge generation and direct d_{31} and d_{33} values as a function of dynamic stress for HMT-SPU and LMT-SPU films, respectively.

2.5. Direct piezoelectric property of various PVDF films for mechanical energy harvesting and sensing

These piezoelectric PVDF films can be used for mechanical energy harvesting and sensing with improved properties. Figs. 9A and B show the charge generation for HMT-SPU and LMT-SPU PVDF films, respectively, in response to the dynamic tensile stresses (T₁). For example, up to 3.65 and 2.60 nC charges could be harvested when the T₁ stresses of 10.41 and 7.01 MPa were applied, respectively (Fig. 9C). From these results, the direct d₃₁ values were calculated as shown in Fig. 9C. For the HMT-SPU film, the direct d₃₁ slightly increased from 36.0 pC/N at 0.52 MPa to 40.3 pC/N at 10.41 MPa. For the LMT-SPU film, the direct d₃₁ slightly increased from 48.5 pC/N at 0.35 MPa to 50.4 pC/N at 7.01 MPa. These direct d₃₁ values were similar to the inverse d₃₁ values at room temperature (see Fig. 6E). In the voltage mode, up to 12.2 and 15.5 V opencircuit voltages were generated for the HMT-SPU and the LMT-SPU PVDF films (Figs. S14A and B), and the generated voltage was linear proportional to the applied tensile stress T₁ (Fig. S14C).

Figs. 9D and E show the charge generation for HMT-SPU and LMT-SPU PVDF films, respectively, in response to the dynamic compression stresses (T₃). For example, up to -0.129 and -0.144 nC charges could be harvested when the applied T₃ were 0.694 MPa, respectively (Fig. 9F). From these results, the direct d₃₃ values were calculated for HMT-SPU and LMT-SPU films, as shown in Fig. 9F. For the HMT-SPU film, the direct d₃₃ was nearly constant around -26.0 pC/N up to 0.7 MPa. For the LMT-SPU film, the direct d₃₃ was almost constant around -28.0 pC/N up to 0.7 MPa. In the voltage mode, up to -0.676 V and -0.840 V open-circuit voltages were generated

for the HMT-SPU and the LMT-SPU samples (Figs. S14A and B), and the generated voltage was linear proportional to the applied compression stress T₃ (Fig. S14C). Based on the above results, the HMT-SPU and LMT-SPU samples had a good mechanical sensing capability.

2.6. Piezoelectric performance of the MMT PVDF samples

To generalize the effect of HHTT defects, we also studied the MMT PDF. As we can see from Fig. S12A, The MMT sample had an Mn of 122.1 Da. The HHTT content was determined to be 5.0 mol.% by ¹H NMR, as shown in Fig. S12B. For the MMT-MR sample, the Tm was 167.4 °C, which was between those of HMT and LMT (Fig. S12C). After uniaxial stretching of the quenched MMT sample, the T_m of the MMT-S sample decreased to 166.1 °C. After electric poling, the T_m was 160.6 °C. Finally, after 20-min high power ultrasonication, the T_m was 160.5 °C. More importantly, the SC heat of fusion increased.

Because of the increased OAF/SC content, the MMT-S also exhibited a peak d₃₁ at 65 C, which coincided with the melting of the SCs. The d₃₁ values were between those of the HMT-SPU and the LMT-SPU samples. This result supports our conclusion that the HHTT defects enabled the formation of OAF and SC_{OAFS} and thus improved the piezoelectric performance of the PVDF homopolymers.

Note that the LMT PVDF has the highest HHTT content as we can obtain from the commercial sources. If we can synthesize PVDF homopolymers with even higher HHTT content, e.g., ~10 mol.%, we expect that even higher piezoelectric performance can be achieved. This work will be reported in the future.

3. Conclusions

In this work, the effects of HHTT defects and high-power ultrasonication on the semicrystalline structure and piezoelectric properties were studied for various HMT and LMT PVDF samples processed under different conditions: stretching/electric poling and stretching/electric poling/ultrasonication. First, the LMT PVDF had a higher HHTT content than the HMT PVDF. Because the HHTT defects were largely expelled from the PC lamellae to form OAF, the LMT PVDF had a lower x_c , but a higher $x_{OAF/SC}$, which was important in enhancing the piezoelectric performance of the PVDF. As a result, the LMT PVDF samples exhibited higher d_{31} values than the HMT PVDF samples. Second, high-power ultrasonication broke nanosized SCs off from the PC lamellae, forming IAF and relaxor-like SC_{OAF}. Due to the enhanced electrostriction from OAF and SC_{OAF}, both LMT and HMT SPU samples exhibited high piezoelectric performance. Third, high thermal stability of piezoelectric performance was achieved: 110 °C for LMT-SPU and 120 °C for HMT-SPU samples.

CRediT authorship contribution statement

Guanchun Rui: Conceptualization, Methodology, Investigation, Formal analysis, Writing – original draft. Elshad Allahyarov: Software, Validation, Writing – review & editing. Honghu Zhang: Data Curation. Ruipeng Li: Data Curation. Shihai Zhang: Resources. Philip L. Taylor: Supervision, Writing – review & editing. Lei Zhu: Project administration, Supervision, Conceptualization, Writing – original draft.

Declaration of Competing Interest

The authors declare that they have no known competing financial interests or personal relationships that could have appeared to influence the work reported in this paper.

Data availability

Data will be made available on request.

Acknowledgment

L.Z. and P.L.T. acknowledge financial support from the National Science Foundation, Division of Materials Research (DMR), Polymers Program (DMR-2103196). E.A. Acknowledges financial support from the Ministry of Science and Higher Education of the Russian Federation (State Assignment No. 075-01129-00).

Appendix A. Supporting information

Supplementary data associated with this article can be found in the online version at doi:10.1016/j.nanoen.2023.xxxxxxxxxxx.

References

- [1] H.S. Nalwa, Ferroelectric Polymers: Chemistry, Physics, and Applications. Marcel Dekker, New York, 1995.
- [2] A.J. Lovinger, Ferroelectric polymers, Science 220(4602) (1983) 1115-1121.
- [3] H. Kawai, Piezoelectricity of poly(vinylidene fluoride), Jpn. J. Appl. Phys. 8(7) (1969) 975-976.
- [4] R. G. Kepler, Ferroelectric, pyroelectric, and piezoelectric properties of poly(vinylidene fluoride). in: H.S. Nalwa (Ed.), Ferroelectric Polymers: Chemistry, Physics, and Applications. Marcel Dekker, Inc., New York, (1995), Chapter 3, pp. 183-232.

- [5] E. Fukada, History and recent progress in piezoelectric polymers, IEEE Trans. Ultrason. Ferroelectr. Freq. Control 47(6) (2000) 1277-1290.
- [6] Q. M. Zhang, C. Huang, F. Xia, J. Su, Electric EAP, in: Y. Bar-Cohen (Ed.), Electroactive Polymer (EAP) Actuators as Artificial Muscles: Reality, Potential, and Challenges. SPIE Press (2004), Chapter 4, pp. 89-139.
- [7] K.S. Ramadan, D. Sameoto, S. Evoy, A review of piezoelectric polymers as functional materials for electromechanical transducers, Smart Mater. Struct. 23(3) (2014) No. 033001.
- [8] Y. Liu, Q. Wang, Ferroelectric polymers exhibiting negative longitudinal piezoelectric coefficient: Progress and prospects, Adv. Sci. 7(6) (2020) No. 1902468.
- [9] M.G. Broadhurst, G.T. Davis, Physical basis for piezoelectricity in PVDF, Ferroelectrics 60(1) (1984) 3-13.
- [10] Y. Huang, G. Rui, Q. Li, E. Allahyarov, R. Li, M. Fukuto, G.-J. Zhong, J.-Z. Xu, Z.-M. Li, P.L. Taylor, L. Zhu, Enhanced piezoelectricity from highly polarizable oriented amorphous fractions in biaxially oriented poly(vinylidene fluoride) with pure β crystals, Nat. Commun. 12(1) (2021) No. 675.
- [11] M.G. Broadhurst, G.T. Davis, J.E. Mckinney, R.E. Collins, Piezoelectricity and pyroelectricity in polyvinylidene fluoride A model, J. Appl. Phys. 49(10) (1978) 4992-4997.
- [12] Y. Wada, R. Hayakawa, A model theory of piezo- and pyroelectricity of poly(vinylidene fluoride) electret, Ferroelectrics 32(1) (1981) 115-118.
- [13] T. Furukawa, J.X. Wen, K. Suzuki, Y. Takashina, M. Date, Piezoelectricity and pyroelectricity in vinylidene fluoride/trifluoroethylene copolymers, J. Appl. Phys. 56(3) (1984) 829-834.

- [14] K. Tashiro, M. Kobayashi, H. Tadokoro, E. Fukada, Calculation of elastic and piezoelectric constants of polymer crystals by a point-charge model Application to poly(vinylidene fluoride) form-I, Macromolecules 13(3) (1980) 691-698.
- [15] T. Wongwirat, Z. Zhu, G. Rui, R. Li, P. Laoratanakul, H. He, H. Manuspiya, L. Zhu, Origins of electrostriction in poly(vinylidene fluoride)-based ferroelectric polymers, Macromolecules 53(24) (2020) 10942-10954.
- [16] Z. Zhu, G. Rui, R. Li, H. He, L. Zhu, Enhancing electrostrictive actuation via strong electrostatic repulsion among field-induced nanodomains in a relaxor ferroelectric poly(vinylidene fluoride-*co*-trifluoroethylene-*co*-chlorotrifluoroethylene) random terpolymer, ACS Appl. Mater. Interfaces 13(35) (2021) 42044-42054.
- [17] T. Furukawa, N. Seo, Electrostriction as the origin of piezoelectricity in ferroelectric polymers, Jpn. J. Appl. Phys. 29(4) (1990) 675-680.
- [18] F. Li, L. Jin, Z. Xu, S. Zhang, Electrostrictive effect in ferroelectrics: An alternative approach to improve piezoelectricity, Appl. Phys. Rev. 1 (2014) No. 011103.
- [19] X. Chen, H. Qin, X. Qian, W. Zhu, B. Li, B. Zhang, W. Lu, R. Li, S. Zhang, L. Zhu, F. Dominguez Dos Santos, J. Bernholc, Q. M. Zhang, Relaxor ferroelectric polymer exhibits ultrahigh electromechanical coupling at low electric field, Science 375(6587) (2022) 1418-1422.
- [20] G. Rui, E. Allahyarov, J. Thomas, P. Taylor, L. Zhu, Temperature-dependent rotational dipole mobility and devitrification of the rigid amorphous fraction in unpoled and poled biaxially oriented poly(vinylidene fluoride), Macromolecules 55 (21)(2022) 9705-9714.

- [21] Y. Liu, H. Aziguli, B. Zhang, W. Xu, W. Lu, J. Bernholc, Q. Wang, Ferroelectric polymers exhibiting behaviour reminiscent of a morphotropic phase boundary, Nature 562(7725) (2018) 96-100.
- [22] Y. Liu, B. Zhang, A. Haibibu, W. Xu, Z. Han, W. Lu, J. Bernholc, Q. Wang, Insights into the morphotropic phase boundary in ferroelectric polymers from the molecular perspective, J. Phys. Chem. C 123(14) (2019) 8727-8730.
- [23] Y. Liu, Z. Han, W. Xu, A. Haibibu, Q. Wang, Composition-dependent dielectric properties of poly(vinylidene fluoride-trifluoroethylene)s near the morphotropic phase boundary, Macromolecules 52(17) (2019) 6741-6747.
- [24] Y. Liu, X. Chen, Z. Han, H. Zhou, Q. Wang, Defects in poly(vinylidene fluoride)-based ferroelectric polymers from a molecular perspective, Appl. Phys. Rev. 9(3) (2022) No. 031306.
- [25] R. Hayakawa, Y. Wada, Piezoelectricity and related properties of polymer films, Adv. Polym. Sci. 11 (1973) 1-55.
- [26] S. Tasaka, S. Miyata, The origin of piezoelectricity in poly(vinylidene fluoride), Ferroelectrics 32(1) (1981) 17-23.
- [27] Y. Wada, Theoretical-analysis of temperature-dependence of complex piezoelectric constant and pyroelectric constant of poly(vinylidene fluoride), Ferroelectrics 57(1) (1984) 343-351.
- [28] P. Harnischfeger, B.J. Jungnickel, Features and origin of the dynamic and the nonlinear piezoelectricity in poly (vinylidene fluoride), Ferroelectrics 109 (1)(1990) 279-284.

- I. Katsouras, K. Asadi, M. Li, T. B. van Driel, K.S. Kjaer, D. Zhao, T. Lenz, Y. Gu, P. W.
 M. Blom, D. Damjanovic, M.M. Nielsen, D.M. de Leeuw, The negative piezoelectric effect of the ferroelectric polymer poly(vinylidene fluoride), Nat. Mater. 15(1) (2016) 78-84.
- [30] G. Rui, Y. Huang, X. Chen, R. Li, D. Wang, T. Miyoshi, L. Zhu, Giant spontaneous polarization for enhanced ferroelectric properties of biaxially oriented poly(vinylidene fluoride) by mobile oriented amorphous fractions, J. Mater. Chem. C 9(3) (2021) 894-907.
- [31] Z. Zhu, G. Rui, Q. Li, E. Allahyarov, R. Li, T. Soulestin, F. Domingues Dos Santos, H. He, P. Taylor, L. Zhu, Electrostriction-enhanced giant piezoelectricity via relaxor-like secondary crystals in extended-chain ferroelectric polymers, Matter 4(11) (2021) 3696-3709.
- [32] Z. Zhu, G. Rui, R. Li, H. He, L. Zhu, Effect of dipole mobility in secondary crystals on piezoelectricity of a poly(vinylidene fluoride-*co*-trifluoroethylene) 52/48 mol % random copolymer with an extended-chain crystal structure, Macromolecules 54(21) (2021) 9879-9887.
- [33] G. Rui, E. Allahyarov, R. Li, P.L. Taylor, L. Zhu, Hard-to-soft transition-enhanced piezoelectricity in poly(vinylidene fluoride) via relaxor-like secondary crystals activated by high-power ultrasonication, Mater. Horizons 9 (2022) 1992-1998.
- [34] H. Ohigashi, K. Omote, T. Gomyo, Formation of single-crystalline films of ferroelectric copolymers of vinylidene fluoride and trifluoroethylene, Appl. Phys. Lett. 66(24) (1995) 3281-3283.
- [35] M.A. Barique, H. Ohigashi, Annealing effects on the Curie transition temperature and melting temperature of poly(vinylidene fluoride/trifluoroethylene) single crystalline films, Polymer 42(11) (2001) 4981-4987.

- [36] T. Hattori, T. Watanabe, S. Akama, M. Hikosaka, H. Ohigashi, The high-pressure crystallization behaviours and piezoelectricity of extended chain lamellar crystals of vinylidene fluoride trifluoroethylene copolymers with high molar content of vinylidene fluoride, Polymer 38(14) (1997) 3505-3511.
- [37] T. Furukawa, Structure and functional properties of ferroelectric polymers, Adv. Colloid and Interface Sci. 71 (2)(1997), 183-208.
- [38] R. Su, J.-K. Tseng, M.S. Lu, M. Lin, Q. Fu, L. Zhu, Ferroelectric behavior in the high temperature paraelectric phase in a poly(vinylidene fluoride-*co*-trifluoroethylene) random copolymer, Polymer 53(3) (2012) 728-739.
- [39] L. Yang, X. Li, E. Allahyarov, P.L. Taylor, Q.M. Zhang, L. Zhu, Novel polymer ferroelectric behavior via crystal isomorphism and the nanoconfinement effect, Polymer 54(7) (2013) 1709-1728.
- [40] T. Hattori, M. Hikosaka, H. Ohigashi, The crystallization behaviour and phase diagram of extended-chain crystals of poly(vinylidene fluoride) under high pressure, Polymer 37(1) (1996) 85-91.
- [41] T. Hattori, M. Kanaoka, H. Ohigashi, Improved piezoelectricity in thick lamellar beta-form crystals of poly(vinylidene fluoride) crystallized under high pressure, J. Appl. Phys. 79(4) (1996) 2016-2022.
- [42] G. Zhang, D. Brannum, D. Dong, L. Tang, E. Allahyarov, S. Tang, K. Kodweis, J.-K. Lee, L. Zhu, Interfacial polarization-induced loss mechanisms in polypropylene/BaTiO₃ nanocomposite dielectrics, Chem. Mater. 28(13) (2016) 4646-4660.
- [43] L. Zhu, Exploring strategies for high dielectric constant and low loss polymer dielectrics,J. Phys. Chem. Lett. 5(21) (2014) 3677-3687.

- [44] G. Zhang, Q. Li, E. Allahyarov, Y. Li, L. Zhu, Challenges and opportunities of polymer nanodielectrics for capacitive energy storage, ACS Appl. Mater. Interfaces 13(32) (2021) 37939-37960.
- [45] K. Mazur, Polymer-ferroelectric ceramic composites, in: H.S. Nalwa (Ed.), Ferroelectric Polymers: Chemistry, Physics, and Applications, Marcel Dekker, Inc., New York, Chapter 11, (1995) pp. 539-610.
- [46] T. Furukawa, K. Ishida, E. Fukada, Piezoelectric properties in the composite systems of polymers and PZT ceramics, J. Appl. Phys. 50(7) (1979) 4904-4912.
- [47] R.E. Newnham, L.J. Bowen, K.A. Klicker, L.E. Cross, Composite piezoelectric transducers, Mater. Design 2(2) (1980) 93-106.
- [48] G.Z. Zhang, P. Zhao, X.S. Zhang, K. Han, T.K. Zhao, Y. Zhang, C.K. Jeong, S.L. Jiang, S.L. Zhang, Q. Wang, Flexible three-dimensional interconnected piezoelectric ceramic foam based composites for highly efficient concurrent mechanical and thermal energy harvesting, Energy Environ. Sci. 11(8) (2018) 2046-2056.
- [49] H.C. Cui, R. Hensleigh, D.S. Yao, D. Maurya, P. Kumar, M.G. Kang, S. Priya, X.Y. Zheng, Three-dimensional printing of piezoelectric materials with designed anisotropy and directional response, Nat. Mater. 18(3) (2019) 234-241.
- [50] R.A. Surmenev, T. Orlova, R.V. Chernozem, A.A. Ivanova, A. Bartasyte, S. Mathur, M.A. Surmeneva, Hybrid lead-free polymer-based nanocomposites with improved piezoelectric response for biomedical energy-harvesting applications: A review, Nano Energy 62 (2019) 475-506.
- [51] G.H. Sessler, R. Gerhard-Multhaupt, Electrets, Laplacian Press, Morgan Hill, CA, (1998)Vol. 1, pp. 1-472.

- [52] P.K.C. Pillai, Polymeric Electrets, in: H.S. Nalwa (Ed.), Ferroelectric Polymers: Chemistry, Physics, and Applications, Marcel Dekker, Inc., New York, Chapter 1, (1995) pp. 1-62.
- [53] L. Zhang, S. Li, Z. Zhu, G. Rui, B. Du, D. Chen, Y.-F. Huang, L. Zhu, Recent progress on structure manipulation of poly(vinylidene fluoride)-based ferroelectric polymers for enhanced piezoelectricity and applications, Adv. Funct. Mater. 33 (2023) DOI: 10.1002/adfm.202301302.
- [54] B. Azimi, M. Milazzo, A. Lazzeri, S. Berrettini, M.J. Uddin, Z. Qin, M.J. Buehler, S. Danti, Electrospinning piezoelectric fibers for biocompatible devices, Adv. Healthc. Mater. 9(1) (2020) No.1901287.
- [55] S. Bauer, R. Gerhard-Multhaupt, G.M. Sessler, Ferroelectrets: Soft electroactive foams for transducers, Phys. Today 57(2) (2004) 37-43.
- [56] B. Ameduri, From vinylidene fluoride (VDF) to the applications of VDF-containing polymers and copolymers: Recent developments and future trends, Chem. Rev. 109(12) (2009) 6632-6686.
- [57] L. Yang, E. Allahyarov, F. Guan, L. Zhu, Crystal orientation and temperature effects on double hysteresis loop behavior in a poly(vinylidene fluoride-*co*-trifluoroethylene-*co*-chlorotrifluoroethylene)-*graft*-polystyrene graft copolymer, Macromolecules 46(24) (2013) 9698-9711.
- [58] X. Chen, E. Allahyarov, Q. Li, D. Langhe, M. Ponting, D. Schuele, E. Baer, L. Zhu, Reducing dielectric loss by nanoconfined impurity ion transport in multilayer films under low electric fields, Compos. Part. B-Eng. 190 (2020) No. 107908.
- [59] X. Chen, E. Allahyarov, D. Langhe, M. Ponting, R. Li, M. Fukuto, D. Schuele, E. Baer, L. Zhu, Reducing dielectric loss and enhancing electrical insulation for multilayer polymer

- films by nanoconfined ion transport under high poling electric fields, J. Mater. Chem. C 8(18) (2020) 6102-6117.
- [60] Z.-Y. Cheng, V. Bharti, T.-B. Xu, S. Wang, Q.M. Zhang, T. Ramotowski, F. Tito, R. Ting, Transverse strain responses in electrostrictive poly(vinylidene fluoride-trifluoroethylene) films and development of a dilatometer for the measurement, J. Appl. Phys. 86(4) (1999) 2208-2214.
- [61] T. Wongwirat, M. Wang, Y. Huang, I. Treufeld, R. Li, P. Laoratanakul, H. Manuspiya, L. Zhu, Mesophase structure-enabled electrostrictive property in nylon-12-based poly(ether-block-amide) copolymers, Macromol. Mater. Eng. 304(9) (2019) 1900330.
- [62] T.R. Shrout, S.J. Zhang, Lead-free piezoelectric ceramics: Alternatives for PZT? J. Electroceram. 19(1) (2007) 113-126.
- [63] M. Kushwah, R. Sagar, A.A. Rogachev, M.S. Gaur, Dielectric, pyroelectric and polarization behavior of polyvinylidene fluoride (PVDF) Gold nanoparticles (AuNPs) nanocomposites, Vacuum 166 (2019) 298-306.